Improved Nerve Cuff Electrode Recordings with Subthreshold Anodic Currents

Mesut Sahin, *Member, IEEE,* and Dominique M. Durand,* *Member, IEEE*

***Abstract*— A method has been developed for improving the signal amplitudes of the recordings obtained with nerve cuff electrodes. The amplitude of the electroneurogram (ENG) has been shown to increase with increasing distance between the contacts when cuff electrodes are used to record peripheral nerve activity [9]. The effect is directly related to the propagation speed of the action potentials. Computer simulations have shown that the propagation velocity of action potentials in a length of a nerve axon can be decreased by subthreshold extracellular anodic currents. Slowing the action potentials is analogous to increasing the cuff length in that both result in longer intercontact delays, thus, larger signal outputs. This phenomenon is used to increase the amplitudes of whole nerve recordings obtained with a short cuff electrode. Computer simulations predicting the slowing effect of anodic currents as well as the experimental verification of this effect are presented. The increase in the amplitude of compound action potentials (CAP's) is demonstrated experimentally in an *in vitro* preparation. This method can be used to improve the signal-to-noise ratios when recording from short nerve segments where the cuff length is limited.**

***Index Terms*— Active membrane models, cable model, compound action potentials, cuff electrodes, extracellular potentials, hyperpolarization, nerve simulation, propagation velocity, whole nerve recording.**

I. Introduction

CUFF electrodes with circumferencial metal contacts have been used to record peripheral nerve activity [1], [2], [5], [6], [10], [11]. The metal contacts are usually configured in the tripolar mode, and therefore, the output signal is the second spatial difference of the extraneural potentials sampled at three different locations along the nerve [9]. The signal output is obtained by taking the difference between the potential waveforms induced by the propagating action potentials at the metal contacts. The amplitude of the signal increases with increasing time delays between the waveforms, i.e., with increasing intercontact distances, and it is proportional to the square of the cuff length [9]. As the distance between the contacts, hence the cuff length is further increased, the signal output reaches a maximum value [10]. Short cuffs can provide sufficiently long delays to achieve the maximum differential signal output when recording from slow fibers. However, the time taken by the action potentials to travel the distance between the contacts of the same electrode is much shorter for a fast fiber, and therefore longer cuffs are required to record maximally from the fast (large) fibers. The maximal available length of the nerve of interest places a limitation on the cuff length in many *in vivo* studies. Moreover, in tripolar configuration, the middle band has to be exactly at the electrical middle point of the nerve impedance between the end contacts in order to eliminate the electromyogram (EMG) contamination from the surrounding muscles into the recordings. In the case of asymmetrical impedances, longer cuffs can produce larger EMG disturbances, in comparison to short cuffs, due to their higher intercontact impedances. Moreover, the Johnson (thermal) noise level increases as the square root of the nerve impedance between the contacts [10], which is proportional to the cuff length. Therefore, it would be very advantageous to use short cuffs for both anatomical and electric noise considerations if the ENG signal amplitudes could be improved.

Computer simulations have shown that low amplitude anodic currents can slow down the propagating action potentials by hyperpolarizing the membrane. Slowing the action potentials is analogous to increasing the cuff length since both result in longer intercontact delays, hence, larger signal outputs. Thus, it should be possible to record from large fibers with a short cuff by decreasing the propagation speed of the action potentials as they pass through the cuff. In this study, the results of the computer simulations predicting the slowing effect of anodic currents as well as the experimental verification of this effect are presented. The increase in the amplitude of recordings made with a short cuff due to extraneural anodic currents is demonstrated with *in vitro* experiments using peripheral nerves. Preliminary data was published in abstract form [7] .

II. Methods

A. Simulations

The effect of subthreshold anodic currents on the propagation of action potentials on a single myelinated axon (diameter $= 10\ \mu$m, length $= 10$ cm) was modeled using the neural simulation software package NEURON [3]. Fig. 1(a) shows the compartmental cable model of the axon. A mammalian model which incorporates voltage gated sodium and leakage channels was used to simulate the active behavior of the cell

Manuscript received January 22, 1997; revised February 24, 1998. This work was supported by the Ministry of National Education of Turkey and by NIH Grant NS 32 845-01. *Asterisk indicates corresponding author.*

M. Sahin is with the Neural Engineering Center, Department of Biomedical Engineering, Case Western Reserve University, Cleveland, OH 44106-4197 USA.

*D. M. Durand is with the Neural Engineering Center, Department of Biomedical Engineering, Case Western Reserve University, Cleveland, OH 44106-4197 USA (e-mail: dxd6@po.cwru.edu).

Publisher Item Identifier S 0018-9294(98)05329-4.

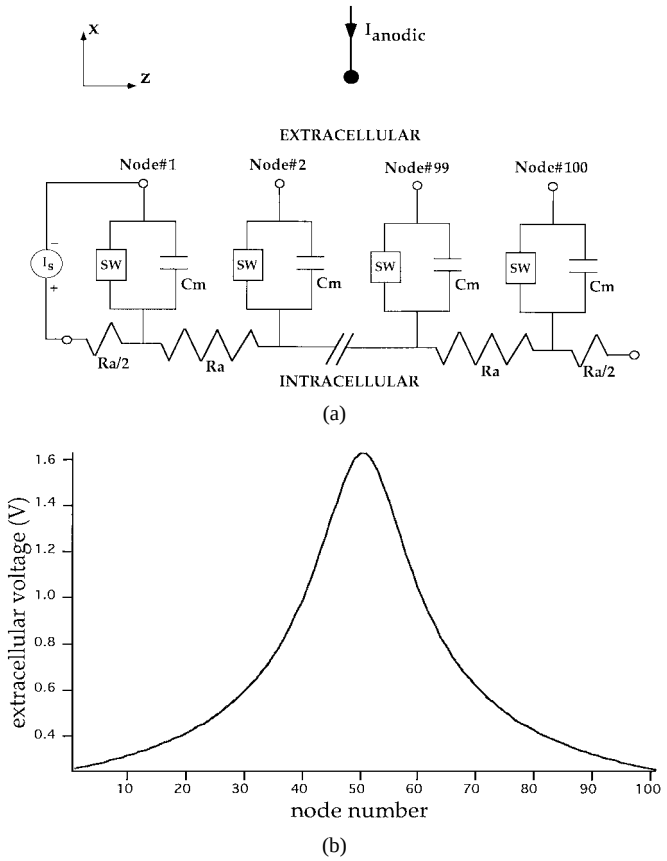

Fig. 1. Axonal simulation. (a) The compartmental cable model of the axon. A mammalian model (SW) is used for the active behavior of the nodal membrane [12]. The passive parameters are: intracellular resistivity = 54.7 Ωcm, membrane capacitance (Cm) = 2.5 μF/cm^2, outer diameter with the myelin sheath = 10 μm, axon diameter = 6 μm, the node length = 1.5 μm, and the internodal distance = 1 mm. (b) Spatial distribution of the extracellular voltage generated by the anodic current source ($I = 300$ mA) located 0.8 cm away from the axon between the nodes 50 and 51 inside an infinite conductive medium ($\sigma^{-1} = 54.7$ Ωcm).

membrane at the nodes of Ranvier [12]. Internodal axoplasmic resistance (Ra) and the nodal transmembrane capacitance (Cm) were lumped into discrete components. An anodic point current source was placed 0.8 cm away from the axon and centered between the nodes 50 and 51. The axon and the anodic current source were placed in an infinite conductive medium.

The extracellular potential field along the axon generated by the anodic current source was computed using the following equation and plotted in Fig. 1(b):

$$\Phi = \frac{I_{\text{anodic}}}{4\pi\sigma\sqrt{x^2 + z^2}} \tag{1}$$

where σ is conductivity of the medium ($\sigma^{-1} = 54.7$ Ωcm), z is the longitudinal axis along the axon, x is the normal distance from the current source to the axon (0.8 cm), and I_{anodic} is the current source amplitude. The distortion of the extracellular field due to the presence of the axon was ignored [4].

NEURON was modified to incorporate the extracellular field by adding an equivalent set of intracellular current sources as previously shown by Warman *et al.* [13]. Discrete current sources proportional to the second order spatial difference of the extracellular voltage profile were applied to the nodes intracellularly while all the nodes were short circuited on the extracellular side.

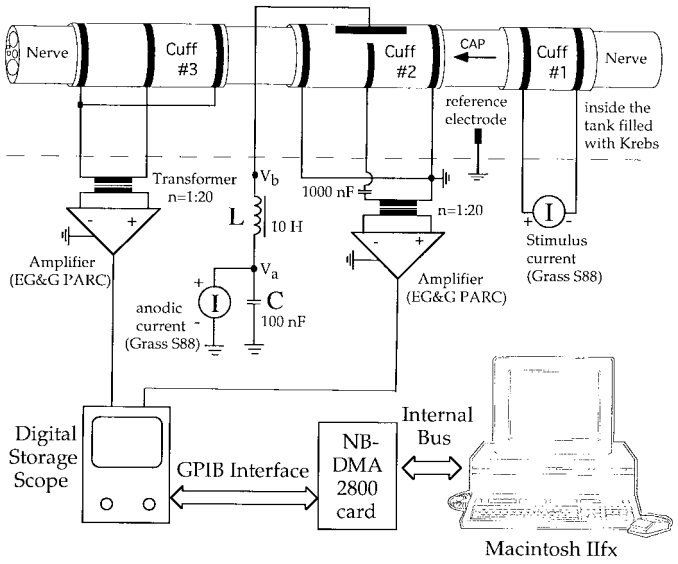

Fig. 2. Experimental setup. The nerve was fitted into the cuff electrodes through longitudinal openings and placed in a 2-l tank filled with Krebs solution. The temperature was kept between 35.5 and 37.5 °C. Three cuff electrodes were placed along the nerve: a stimulation cuff (Cuff#1, contact separation is 3 mm), an anodic current and recording cuff (Cuff#2, three bands with a 3-mm separation between each and a longitudinal metal contact that is 3×1 mm), and another recording cuff (Cuff#3, three bands with 3-mm separations). Both Cuff#2 and Cuff#3 were configured in the tripolar mode for recording.

A stimulation pulse ($I_s = 20$ nA, 10 μs) was applied at the first node at time equal to zero. The temporal waveform of the transmembrane voltage was computed at each node as the action potential propagated along the axon. Local propagation velocities were calculated by taking the reciprocal of the time interval between the action potential peaks at consecutive nodes. The additional delay generated by the injection of extracellular anodic current was defined as the anodic delay.

B. Experiments

1) In Vitro Recording Setup: In vitro experiments were conducted by placing a nerve and three cuff electrodes (inner diameter = 0.76 mm) in a tank filled with Krebs solution (pH = 7.4) with temperature maintained between 35.5–37.5 °C (Fig. 2). Ten nerves (eight pig phrenic, one pig vagus, and one rat sciatic) were tested with various cuff designs to demonstrate the slowing effect of the anodic currents. The nerves were dissected and placed in the recording chamber immediately. A gas mixture of 95% oxygen and 5% carbon dioxide was bubbled through the solution for oxygenation of the nerve. Three different cuff electrodes were placed along the nerve. These cuff electrodes were fabricated manually using silicone tubing and platinum foil contacts that were fixed on the inner surface of the tubing and were soldered to lead wires for electrical connection. The first cuff (Cuff#1) had two circumferencial platinum band contacts located 3 mm apart and was used for stimulation of the nerve. The second cuff (Cuff#2) had three bands with 3 mm separations between

each and a 3×1 mm longitudinal contact. The middle band was not a complete circle leaving 1-mm gaps on each side of the longitudinal contact. This cuff was used to apply a subthreshold anodic current to the nerve to slow down the action potentials and also to record the compound action potentials (CAP's). The third cuff (Cuff#3) had three full circle bands with 3 mm separations and was used to measure the propagation delay of the CAP's. All the platinum band contacts were 1-mm wide and 50 μm in thickness. All the cuffs had slits along their lengths to allow the nerve to be fitted inside the cuffs. The openings and the ends of the cuffs were sealed with petroleum jelly before the preparation was bathed into the Krebs solution. A reference electrode was placed in the tank at a distance from the cuff electrodes and connected to the electronic ground. The recordings began within 2 h of the nerve dissection and very high signal-to-noise ratios (SNR's) were obtained for at least 3–6 h.

Two hypotheses were tested with the experiments: 1) the propagation velocity of the action potentials can be lowered by extracellular anodic currents as predicted by the computer simulations, 2) the action potential amplitudes recorded with a short cuff (Cuff#2) increase as a result of the decrease in the propagation velocity taking place inside the cuff.

The propagation delay was estimated from the Cuff#3 recordings and defined as the time interval between the stimulation pulse and the time when the CAP's crosses the zero line from positive to negative [the waveform with no anodic current $T(0\ \mu\text{A})$ in Fig. 6(a)]. The anodic delay was defined as the additional delay generated by the anodic current, and is given by

$$\text{anodic delay} = T(I_{\text{anodic}}) - T(I_{\text{zero}}) \tag{2}$$

where $T(I_{\text{anodic}})$ is the propagation delay for the anodic current value of I_{anodic} and $T(I_{\text{zero}})$ is the propagation delay without the anodic current. The amplitudes of the CAP's from Cuff#2 were computed using the following:

$$V_{\text{CAP}} = V_{\max} - \frac{V_{\min} - V_{\min 2}}{2} \tag{3}$$

where $V_{\max}$ is the positive peak, $V_{\min 1}$ is the first negative peak, and $V_{\min 2}$ is the second negative peak of the triphasic CAP waveform [see Fig. 6(b)].

The percent increase in the CAP for a given anodic current amplitude is defined as

$$\%\text{increase}\,(I_{\text{anodic}}) = \frac{[V_{\text{CAP}}(I_{\text{anodic}}) - V_{\text{CAP}}(I_{\text{zero}})]}{V_{\text{CAP}}(I_{\text{zero}})} \times 100. \tag{4}$$

The recording electronics for each channel consisted of an audio transformer (turn ratio $= 1:20$, Part # 24400, PICO Electronics), a commercial preamplifier (Model 113, EG&G PARC) with a built in Band-Pass filter (300 Hz–10 KHz), and a digital storage oscilloscope (Tektronix 2230–100 MHz). A DMA board (NB-DMA2800, National Instruments) and a data acquisition software (Labview, National Instruments) were used to transfer the acquired CAP's from the digital storage oscilloscope to a Macintosh IIfx computer. Each trace consisted of 512 data points sampled at 4- or 10-μs time intervals.

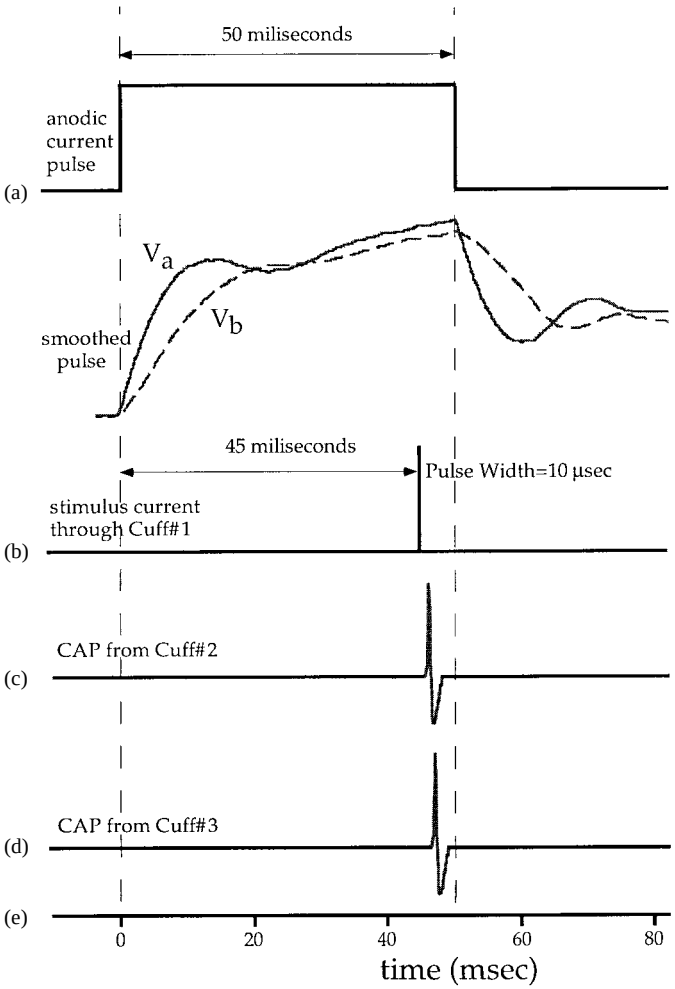

Fig. 3. Temporal relation between the stimulus pulse and the recorded waveforms in the experimental setup. (a) Anodic current pulse, (b) voltages V_a and V_b in Fig. 2, showing that the edges of the anodic current are smoothed by the low-pass filter consisting of an inductor (10 H @ 60 Hz) and a capacitor (100 nF), (c) stimulus current; pulse width was set to 10 μs and the amplitude was set a value between 50 μA–1.5 mA for all the nerves, (d) CAP recorded from Cuff#2, and (e) CAP recorded from Cuff#3. The voltage waveforms V_a and V_b do not return to zero immediately after the anodic pulse is turned off because of the charge remained on the contact capacitance. Sufficiently long time intervals were allowed for this capacitance to discharge before the next anodic pulse was applied.

A Grass S88 stimulator was used to generate both the stimulus and anodic current pulses [Fig. 3(a) and (c)]. A low-pass filter consisting of an inductor (10 H @ 60 Hz) and a capacitor (100 nF) was used for smoothing the edges of the anodic pulse to reduce the artifact in the recordings [Fig. 3(b)]. An interval of 45 ms between the onset of the anodic current pulse and the stimulus pulse was allowed for the outputs of the pre-amplifiers to stabilize after the onset of the anodic pulse.

C. Experimental Protocol

The nerve was stimulated with a rectangular current pulse (10 μs, 50 μA–1.5 mA). The amplitude of the anodic current was first raised from 0 μA to a maximal value (110–150 μA) then lowered back to 0 μA in predetermined steps while

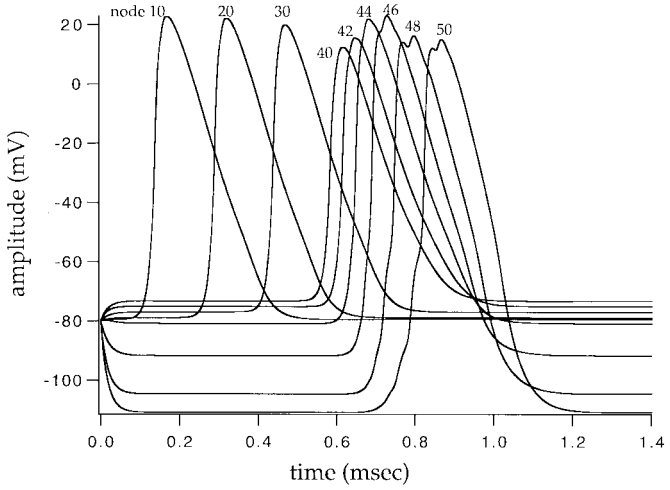

Fig. 4. Simulated action potential waveforms shown at nodes 10, 20, 30, 40, 42, 44, 46, 48, and 50. The temporal resolution of the plots is 1 μs. Note that the peak amplitudes are increased for the hyperpolarized nodes (46, 48, and 50) and decreased for the depolarized nodes (30, 40, and 42).

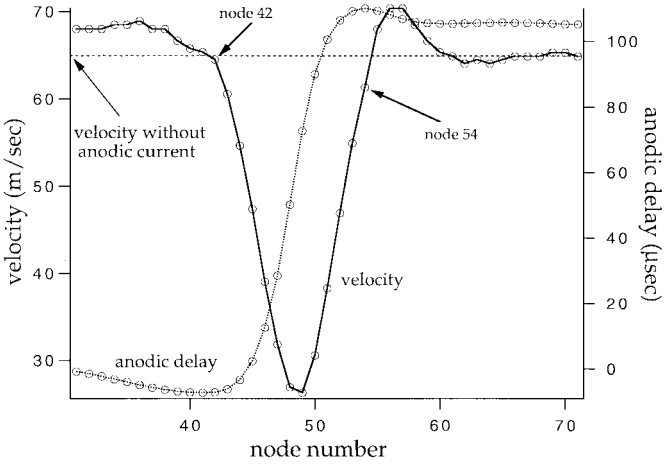

Fig. 5. Simulated local conduction velocities and the anodic delay values at the nodes of the axon model shown in Fig. 1(a). The propagation velocity without extracellular anodic current was 64.73 m/s. Only the values between the nodes 31 and 71 are shown.

CAP's from Cuff#2 and Cuff#3 were recorded and stored into the computer. This procedure was repeated four to six times $(N = 4 - 6)$ within 30–90 min. Anodic delays, CAP amplitudes, and percent increases in the CAP amplitudes were computed for each acquisition. The mean and standard deviations were calculated for the data points obtained from the same nerve at corresponding anodic current values.

III. Results

A. Computer Simulations

The axon model shown in Fig. 1(a) was stimulated at node #1 with no extracellular anodic source resulting in the generation of an action potential propagating at the velocity of 64.73 m/s. An anodic current source (300 mA) located 0.8 cm away from the axon between nodes 50 and 51 was then applied at time $t = 0$ generating the extracellular potential field shown in Fig. 1(b) along the axon. The resulting action potentials computed at several nodes are shown in Fig. 4 to demonstrate the effect of the anodic current on the resting membrane potentials (initially set to -80 mV), the peak amplitudes, and the propagation velocity. The anodic current hyperpolarizes the nodes closer to the electrode (nodes 44–56) and depolarizes the others. The nodal transmembrane potentials reach their new value and stabilize shortly after the onset of the anodic current (within 70 μs). The fact that no action potential is produced at the most depolarized node immediately after the anodic current is applied shows that the anodic current amplitude is subthreshold. The amplitudes of the action potentials are increased at the hyperpolarized nodes (46, 48, and 50) and decreased at the depolarized nodes (30, 40, and 42). There is also a decrease in the slope of the rising edge of the action potentials at the most hyperpolarized nodes (by 4%, 29%, and 48% at nodes 46, 48, and 50, respectively). The local propagation velocities computed at the nodes of Ranvier are plotted in Fig. 5. The velocity is maximally reduced at node #49 by 59% of its original value, i.e., the velocity without the anodic current. The anodic delay values computed along the nerve are also shown in Fig. 5. The propagation delay between the nodes 42 and 54 increased from 185–302 μs when the anodic current is applied. Therefore, the application of the anodic current increased the propagation delay by 63% within this segment of the axon. These simulation results suggest that it should be possible to slow down the propagation of action potentials by applying subthreshold anodic currents.

B. Experimental Results

Different cuff designs provided different degrees of anodic current effect (see discussion). The slowing down effect and the increase of the CAP amplitudes with the anodic currents have been observed with all the working cuff designs and nerves. Here, we present data from experiments carried out with the cuff design shown in Fig. 2. Four nerves, three phrenic nerves from pigs (2.5–5 kg), and one rat sciatic nerve were used. A typical set of CAP's recorded from Cuff#3 from a pig phrenic nerve following electrical stimulation (50 μA, 10 μs, applied through Cuff#1) is shown in Fig. 6(a) for various amplitudes of the anodic current (applied through Cuff#2). The arrival time of the CAP is delayed indicating that the propagation velocity is reduced by the anodic current (hypothesis 1). As the current is increased above 100 μA, the amplitude of the CAP starts to decrease. This may be due to the fact that some fibers are blocked by the anodic current [8]. Blocking was evident at larger anodic currents and it was possible to annihilate the entire CAP signal by increasing the anodic current amplitude further.

The CAP's recorded from Cuff#2 simultaneously with those from Cuff#3 are plotted in Fig. 6(b). This figure shows that the CAP amplitude recorded from a short cuff (Cuff#2) increases with increasing anodic current amplitudes (hypothesis 2). The CAP amplitude for zero anodic current is small (144 μV) due to the small separation between the contacts (3 mm). As the anodic current amplitude is raised, a greater number of fibers are slowed down and begin to contribute to the signal. The maximum output (450 μV) in this data set is obtained for the

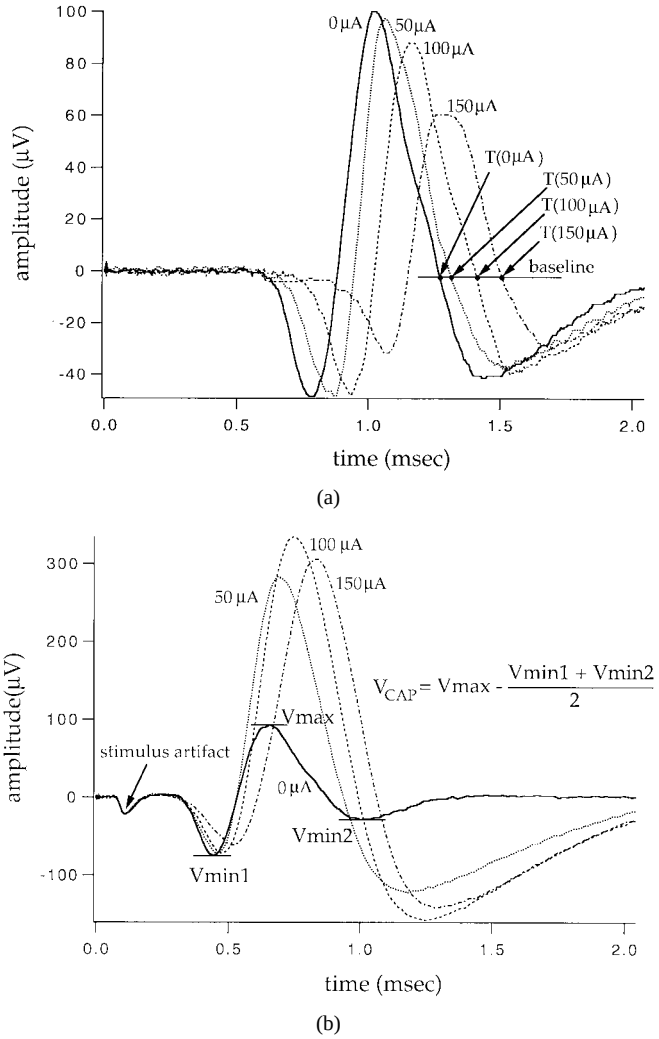

Fig. 6. CAP's recorded from a pig phrenic nerve for the anodic current values of 0, 50, 100, and 150 μA. (a) CAP's recorded from Cuff#3 are delayed by the anodic current indicating that the propagation velocity is reduced within Cuff#2 (hypothesis 1). The propagation delays are denoted as $T(I_{\mathrm{anode}})$ for each anodic current level. (b) Recordings obtained from Cuff#2 simultaneously with those in (a). This figure demonstrates that the CAP amplitude recorded from a short cuff (Cuff#2) is increased with increasing anodic currents (hypothesis 2). The points at which the measurements are taken to calculate the CAP amplitudes [see (3)] are marked on one of the waveforms.

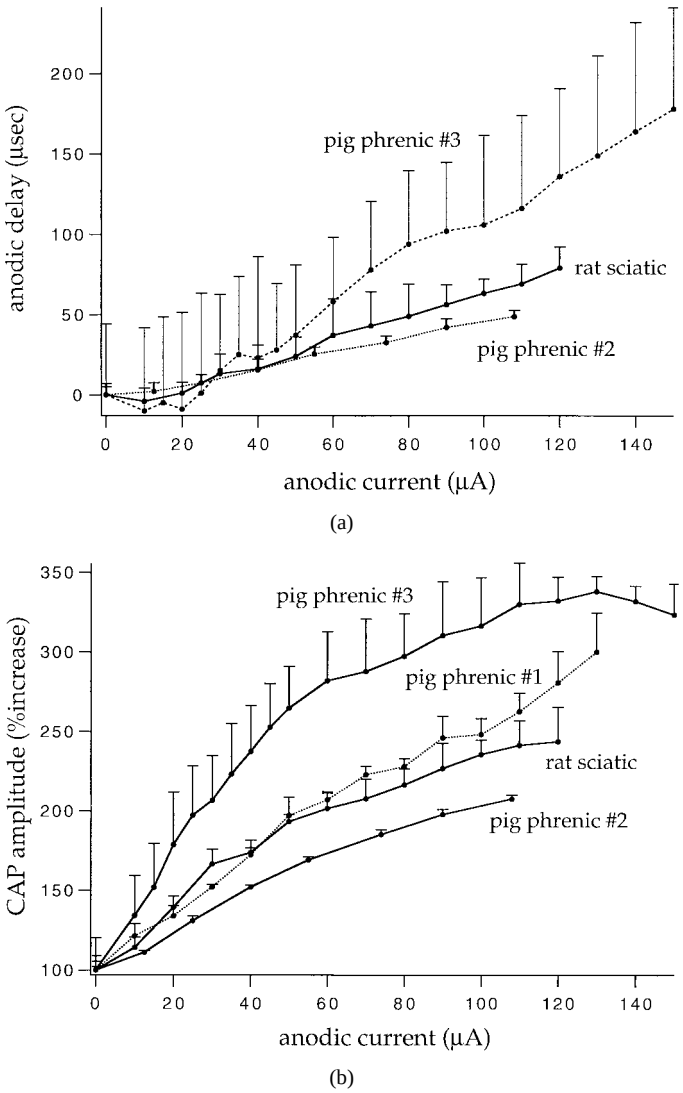

Fig. 7. Mean anodic delay generated within Cuff#2 and the mean percent increases in the CAP amplitudes from the same cuff versus the anodic current (see Methods). Standard deviations (+SD) are also shown. (a) Mean anodic delays for the pig phrenic #2 ($N = 6$), the pig phrenic #3 ($N = 4$), and the rat sciatic ($N = 4$) nerves. (b) Mean percent increases in the CAP amplitudes for the pig phrenic #1 ($N = 6$), the pig phrenic #2 ($N = 6$), the pig phrenic #3 ($N = 4$), and the rat sciatic ($N = 4$) nerves. The percent increases are computed relative to the CAP amplitudes acquired without the anodic current [see (4)].

anodic current value of 100 μA. Further increases in the anodic current causes the CAP amplitude to decay.

The mean values of the anodic delay are plotted as a function of the anodic current for the pig phrenic nerves #2 and #3 and the rat sciatic nerve in Fig. 7(a). The delay increases with increasing anodic current after an initial plateau. The mean percent increases in the CAP amplitudes from Cuff#2 for the same nerves in addition to that of the pig phrenic nerve #1 are plotted in Fig. 7(b) as a function of the anodic current. There is a steady increase in the CAP amplitudes with increasing values of the anodic current. The maximum percent increases in the amplitudes of CAP's are 108, 144, 200, and 238% for the pig phrenic #2, the rat sciatic, the pig phrenic #1, and the pig phrenic #3 nerves at the anodic current values of 108, 120, 130, and 130 μA, respectively. The mean values of the anodic delay for these increases in the CAP amplitudes are 49 μs for the pig phrenic #2, 79 μs for the rat sciatic, and 175 μs for the pig phrenic #3 nerves. Although the CAP amplitudes were readily available for all the nerves, the anodic delay measurements from the pig phrenic #1 were not included since the noise level did not allow accurate delay measurements. The percent increases of the CAP amplitudes are larger for the nerves for which larger anodic delays are obtained. No excitation of the nerve with the anodic current pulse was observed even at the anodic current amplitudes that provided the maximal increases in the CAP amplitudes.

IV. Discussion

The data presented here shows that it is possible to reduce the propagation velocity of action potentials using subthreshold anodic currents. Computer simulations show that the

propagation velocity is decreased when the axon is hyperpolarized by the applied current. A possible mechanism underlying this effect is that the hyperpolarizing currents from the anodic source cancels out a fraction of the depolarizing currents generated by the preceding nodes, and therefore it takes a longer time to bring the next node to the activation threshold. Another mechanism by which the slowing down effect can occur is through the decrease in the slope of the rising edge of the action potentials due to hyperpolarization. In either case, the anodic delay effect should take place shortly after the onset of the anodic current. A minimum delay of 25 ms was required in these experiments, but this delay was attributed to the long time constant of the low-pass filter used (including the nerve impedance) to reduce the artifact generated in the recording amplifier by the rising edge of the anodic current. Therefore, it should be possible to use shorter anodic pulse durations by removing the artifact with a blocking circuitry placed before the recording amplifier [6].

Interestingly, the minimum velocity peak in Fig. 5 is shifted toward the left by two nodes with respect to the maximum value of the extracellular voltage which is between the nodes 50 and 51. Moreover, the velocity curve is asymmetric relative to the negative peak. The shift and the asymmetry in this plot can only result from the directionality introduced by the propagation of the action potentials, which is from left to right. A possible explanation for these effects is as follows: the amplitudes of action potentials increase at the hyperpolarized nodes and decrease at the depolarized nodes as, shown in Fig. 4. These variations in the action potential amplitudes result in an additional complexity because the activation latency is not only determined by how much hyperpolarizing or depolarizing current a given node experiences but also by the action potential amplitudes of the preceding nodes that activate that node. The activation time of a node is maximum if the node is hyperpolarized but preceded by nodes that are depolarized. Considering the two corresponding nodes on each side of the central node, the left one has a larger activation latency since it is preceded by the nodes that are depolarized. Since this effect takes place at all the nodes, the velocity curve is shifted toward the left with respect to the center node and is asymmetrical relative to its negative peak.

The experiments verified the predictions of the computer simulations that the extraneural anodic currents reduce the propagation velocity. In the simulations, the total anodic delay for the axon segment between the nodes 42 and 54 was 117 μs, which corresponds to 9.75 μs per millimeter of the axon. The maximum anodic delay values obtained with the experiments using a 6-mm cuff ranged between 49–175 μs, which corresponds to 8–29 μs per millimeter of the nerve inside the cuff. This wide range of the anodic delays can be explained by the differences in the sizes of the fibers being stimulated. For the same percent changes in the velocity, different anodic delays are generated if the original propagation velocities, i.e., the sizes of the fibers, are different.

Several designs for Cuff#2 were tested to maximize the anodic delay. In an early design, the longitudinal contact was divided into two halves and placed on each side of the middle band that was used for recordings [7]. In an effort to eliminate the longitudinal contact, the middle band of the cuff was used to deliver the anodic current. But, this method did not provide significant anodic delays, suggesting that a minimum length for the longitudinal contact is required to effectively decrease the velocity. A longer cuff with the same intercontact distance (2×3 mm) was very effective for obtaining large anodic delays. However, this design was abandoned since the design did not satisfy our original criteria for minimizing cuff length. The current design was found to give the largest anodic delays and increases in the CAP amplitudes with a short cuff (6 mm).

The percent increases obtained in the signal amplitude and the anodic current values required for these increases were variable from preparation to preparation. However, in all preparations there was always an increase in the signal amplitude when the anodic current was applied [Fig. 7(b)]. A small percentage of the increase can be attributed to the increase in the amplitude of the action potentials at the hyperpolarized nodes of Ranvier, as was observed with the simulations (see Fig. 4). However, this effect cannot account for signal increases as large as 238%. It is suggested that the main factor for the signal increase must be the increase in the delay between the contacts under anodic currents, which is analogous to increasing the cuff length.

The amplitude of the CAP's recorded with Cuff#3 start to decrease before the Cuff#2 recordings are maximally increased by the anodic current. As shown in Fig. 6, the CAP's recorded from Cuff#3 are slightly decreased in amplitude for an anodic current amplitude of 100 μA although the CAP amplitude from Cuff#2 is at maximum for the same anodic current value. This decrease in the amplitudes recorded from Cuff#3 could be explained by the fact that some fibers are being blocked by the anodic current [8]. Another possible explanation is that there is temporal cancellation between the positive and negative phases of the action potentials from different fibers. Because the fibers have different sizes and are located at various distances from the contact, the anodic current generates different amounts of delay in each one of them. The larger and the closer fibers are delayed more than others. Negative and positive phases of action potentials from various fibers can cancel each other out as a result of this effect. It is not possible to differentiate between the two factors. The blocking effect is probably not substantial for a large range of anodic current values after the Cuff#3 recordings begin to decrease since the CAP amplitude from Cuff#2 continue to rise with increasing anodic currents. Notice also that due to the reasons mentioned above, the shape of the CAP's is modified by the anodic current [Fig. 6(b)]. However, this should not present a problem for most nerve recording applications using the cuff electrodes since the cuff electrodes function like a linear filter in the frequency domain and modify the shape of CAP's even in the absence of the anodic currents. In these applications, it is usually the amount of activity or the presence of activity that is used as the information source [1], [2], [6].

The large increase in the CAP amplitudes with even small amplitudes of the anodic current suggest that this method could be used to improve the SNR of nerve recordings. The nerve cuff recordings usually have low signal amplitudes unless very long cuffs are used [1], [2], [6], [10], [11]. This method can

be used as a tool to improve the quality of nerve recordings when noise presents a problem. One can chose a very short cuff to minimize the Johnson (thermal) noise, but still record as large signals, as can be recorded with long cuffs. This method can also make it possible to record from short nerve branches with good SNR where the cuff length is limited. Another potential application of the technique is selective whole nerve recordings. By specifically hyperpolarizing a local cluster of fibers (e.g., a fascicle) in the nerve trunk, one can amplify the signals recorded only from that cluster excluding the others.

V. Conclusions

Computer simulations predict that the propagation velocity of action potentials can be decreased by using subthreshold anodic currents. Experimental data verified the simulations and also demonstrated that the compound action potential amplitudes recorded with a short cuff can be increased up to three times as a result of this reduction in velocity. The data suggest that this method can be used to improve the SNR of nerve recordings.

Acknowledgment

The authors would like to express their gratitude to Dr. I. A. Dreshaj for providing the nerves.

References

[1] M. K. Haugland and T. Sinkjær, "Cutaneous whole nerve recordings used for correction of footdrop in hemiplegic man," *IEEE Trans. Rehab. Eng.*, vol. 3, pp. 307–317, Dec. 1995.

[2] M. K. Haugland and J. A. Hoffer, "Slip information provided by nerve cuff signals: Application in closed-loop control of functional electrical stimulation," *IEEE Trans. Rehab. Eng.*, vol. 2, pp. 29–36, Mar. 1994.

[3] M. Hines, "A program for simulation of nerve equations with branching geometries," *Int. J. Biomed. Comput.*, vol. 24, pp. 55–68, 1989.

[4] D. R. McNeal, "Analysis of a model for excitation of myelinated nerve," *IEEE Trans. Biomed. Eng.*, vol. BME-23, pp. 329–336, Mar. 1976.

[5] Z. M. Nikolic, D. B. Popovic, R. B. Stein, and Z. Kenwell, "Instrumentation for ENG and EMG recordings in FES systems," *IEEE Trans. Biomed. Eng.*, vol. 41, pp. 703–706, July 1994.

[6] D. B. Popovic, R. B. Stein, K. L. Jovanovic, R. Dai, A. Kostov, and W. W. Armstrong, "Sensory nerve recording for closed-loop control to restore motor functions," *IEEE Trans. Biomed. Eng.*, vol. 40, pp. 1024–1030, Oct. 1993.

[7] M. Sahin and D. M. Durand, "Improved nerve cuff electrode recordings by subthreshold anodic currents," in *Proc. IEEE 17th Ann. Conf. Eng. Med. Biol. Soc.*, 1995.

[8] M. Sassen and M. Zimmermann, "Differential blocking of myelinated nerve fibers by transient depolarization," *Pflugers Arch.*, vol. 341, no. 3, pp. 179–195, 1973.

[9] R. B. Stein and K. G. Pearson, "Predicted amplitude and form of action potentials recorded from unmyelinated nerve fibers," *J. Theor. Biol.*, vol. 32, pp. 539–558, 1971.

[10] R. B. Stein, D. Charles, L. Davis, L. Jhamandas, A. Mannard, and T. R. Nichols, "Principles underlying new methods for chronic neural recording," *Can. J. Neur. Sci.*, Aug. 1975, pp. 235–244.

[11] R. B. Stein, T. R. Nichols, J. Jhamandas, L. Davis, and D. Charles, "Stable long-term recordings from cat peripheral nerves," *Brain Res.*, vol. 128, pp. 21–38, 1977.

[12] J. D. Sweeney, J. T. Mortimer, and D. Durand, "Modeling of mammalian myelinated nerve for functional neuromuscular stimulation," in *Proc. IEEE 9th Ann. Conf. Eng. Med. Biol. Soc.*, vol. 1577, 1987.

[13] E. Warman, W. M. Grill, and D. Durand, "Modeling the effects of electric fields on nerve fibers: Determination of excitation threshold," *IEEE Trans. Biomed. Eng.*, vol. 40, pp. 1175–88, 1993.

Mesut Sahin (S'95–M'97) received the B.S. degree in electrical engineering from Istanbul Technical University, Turkey, in 1986, and the M.S. degree in biomedical engineering from Case Western Reserve University (CWRU), Cleveland, OH, in 1992. He received the Ph.D. degree in biomedical engineering from CWRU in 1998.

He was with TELETAS A.S., Istanbul, Turkey, from 1987 to 1990, working as a Research and Development Engineer. He is currently a Research Associate in the Neural Engineering Center at CWRU. His research interests are in nerve recording techniques in general and particularly in sleeping animals for studying "obstructive sleep apnea."

Dominique M. Durand (M'91) was born in Monbazillac, France, in 1951. He received the Engineering degree from Ecole Nationale Superieure d'Electronique, Hydrolique, Informatique et Automatique de Toulouse, France, in 1973. In 1974, he received the M.S. degree in biomedical engineering from Case Western Reserve University (CWRU), Cleveland, OH, and in 1982 he received the Ph.D. degree in electrical engineering from the Institute of Biomedical Engineering, University of Toronto, Toronto, Ont., Canada.

He was with the Addiction Research Foundation of Toronto, Toronto, Ont., Canada, for several years and is currently a Professor in the Departments of Biomedical Engineering and Neurosciences at CWRU. His research interests are in neural engineering, which includes computational neuroscience, neurophysiology, nonlinear dynamics of neural systems, neural prostheses, and magnetic and electrical field interactions with neural tissue.

Dr. Durand has received an NSF Young Investigator Presidential Award as well as undergraduate and graduate teaching awards.